Geosci. Model Dev., 7, 725–736, 2014
www.geosci-model-dev.net/7/725/2014/
doi:10.5194/gmd-7-725-2014

Geoscientific Model Development
Open Access

Snow water equivalent modeling components in NewAge-JGrass

G. Formetta[1], S. K. Kampf[2], O. David[3], and R. Rigon[1]

[1]University of Trento, 77 Mesiano St., 38123 Trento, Italy
[2]Dept. of Ecosystem Science and Sustainability, Colorado State University, Fort Collins, CO, USA
[3]Dept. of Civil and Environmental Engineering, Colorado State University, Fort Collins, CO, USA

Correspondence to: G. Formetta (giuseppe.formetta@unical.it)

Received: 16 July 2013 – Published in Geosci. Model Dev. Discuss.: 30 August 2013
Revised: 14 March 2014 – Accepted: 17 March 2014 – Published: 6 May 2014

Abstract. This paper presents a package of modified temperature-index-based snow water equivalent models as part of the hydrological modeling system NewAge-JGrass. Three temperature-based snow models are integrated into the NewAge-JGrass modeling system and use many of its components such as those for radiation balance (short wave radiation balance, SWRB), kriging (KRIGING), automatic calibration algorithms (particle swarm optimization) and tests of goodness of fit (NewAge-V), to build suitable modeling solutions (MS). Similarly to all the NewAge-JGrass components, the models can be executed both in raster and in vector mode. The simulation time step can be daily, hourly or sub-hourly, depending on user needs and availability of input data. The MS are applied on the Cache la Poudre River basin (CO, USA) using three test applications. First, daily snow water equivalent is simulated for three different measurement stations for two snow model formulations. Second, hourly snow water equivalent is simulated using all the three different snow model formulae. Finally, a raster mode application is performed to compute snow water equivalent maps for the whole Cache la Poudre Basin.

1 Introduction

The physically based approach is the most complete method of simulating snowpack evolution. This solution has reached maturity and was pursued successfully with many recent models including CROCUS (Brun et al., 1992), Alpine3D (Lehning et al., 2006), GEOtop (Rigon et al., 2006; Endrizzi et al., 2013; Endrizzi, 2007; Dall'Amico et al., 2011), ISNOBAL (Marks et al., 1999) and Utah energy balance model (UEB) (Tarboton et al., 1996). These models simulate snow accumulation and ablation using the energy budget and may also include ancillary modeling of blowing snow and other features required to reproduce the full set of thermodynamic quantities representative of snowpack state. However, simpler models tend to be preferred to complex ones because the latter require much more detailed information (in time and in space) regarding model input and model parameter values. Moreover real-time modeling with data assimilation and parameter calibration may require that a forecasting simulation be generated within a few minutes, and this can be accomplished only with simpler models. Simpler models, however, are usually limited to forecasting just the snow water equivalent (SWE, the mass of liquid water in the snowpack) and not other variables such as snow depth and density. One early example of a simple snow accumulation and ablation model is the snowmelt runoff model (SRM) by Martinec (1975). This model was applied to hundreds of basins with reasonable success (Martinec et al., 1983, 1994). SRM is a linear model in which the independent variables are average daily temperature and an estimate of the catchment area covered by snow. The snow-covered area can be determined from airborne or satellite remote sensing data, and loss of snow cover is then simulated based on a temperature index. Simulations are typically run at a daily time step.

For example, in Cazorzi and Dalla Fontana (1996) and Hock (1999) the radiation term is an energy index computed for each pixel of the grid as shortwave solar radiation integrated over a time period that is longer than the model time step, as explained in Sect. 2. In Hock (1999) the melt factor depends on the value of the clear-sky solar radiation, following studies by Kustas et al. (1994) and Brubaker et al. (1996). Hock's model depends on two separate terms: a constant value (melt coefficient) and a value function of the

potential solar radiation (radiation coefficient) computed for every time step. A third temperature-based snow modeling approach was presented by Tobin et al. (2013), who proposed to use a varying degree-day factor throughout the day to improve simulation of snowmelt rates at sub-daily time steps as a component of a runoff model.

In this paper we implement three of these temperature-based snow models: a temperature index (C1), Cazorzi and Dalla Fontana's model (C2) and Hock's model (C3) of snow water equivalent, which estimates SWE from spatially distributed radiation and temperature. The snow models are provided as components of the object modeling system version 3 framework (OMS3; David et al., 2013) and integrated with the others into the NewAge-JGrass system (Formetta et al., 2011, 2013; Formetta, 2013). The system is able to model hydrologic fluxes using various alternative configurations (called modeling solutions, MS) for each process. The purpose of this paper is to illustrate how the SWE models can be implemented as model solutions without changing the ancillary tools when switching from one SWE MS to the other. The model components can then be executed using OMS3 implicit parallelism to improve computational efficiency in multicore or multiprocessor machines. The paper is organized as follows: Sect. 2 presents the models' equations; Sect. 3 contains a general description of the NewAge-JGrass system; and Sect. 4 contains a test of the model for an example basin.

2 The NewAge-SWE component

The snow water equivalent modeling components in NewAge are built following the conceptual scheme presented in Kokkonen et al. (2006), varying the contents of the snowpack mass balance equation. In particular the new additions are as follows:

- Snowmelt is simulated with three different temperature-based solutions.
- The separation of rain from snow precipitation uses a smoothing function based on air temperature rather than a threshold air temperature. This approach addresses problems found in prior research by Kavetski et al. (2006), who found that threshold temperatures for precipitation could generate extremely non-smooth parameter surfaces during automatic calibration procedures.

In the next subsection the main algorithms of the model are described in more detail.

Mass balance

The snowpack mass balance is computed as follows. For the solid water content (M_i [mm])

$$\frac{\mathrm{d}M_i}{\mathrm{d}t} = P_\mathrm{s} + F - M \tag{1}$$

and for liquid water (M_w [mm]) in the snowpack

$$\frac{\mathrm{d}M_\mathrm{w}}{\mathrm{d}t} = P_\mathrm{r} - F + M. \tag{2}$$

Equation (1) represents time-varying solid water content in the snowpack as the sum of snowfall, P_s, and freezing water, F, minus melt, M (all expressed as snow water equivalent). Equation (2) represents time-varying liquid water in the snowpack as the sum of the rainfall, P_r, and melt water minus freezing water. If liquid water M_w exceeds liquid water-retention capacity of the snowpack (M_max [mm]), the surplus becomes snowmelt discharge q_m [mm t^{-1}], where t stands for unit of time (hour or day). The liquid water retention capacity of a snowpack is related to the ice content by a linear relationship depending on the coefficient α_l [–], as in Eq. (3):

$$M_\mathrm{max} = \alpha_\mathrm{l} \cdot M_i. \tag{3}$$

Kokkonen et al. (2006) computed these mass balance equations at a daily time step, but here the time step can vary depending on the time resolution of input data.

2.1 Type of precipitation

The first hydrological process simulated is the discrimination between rainfall and snowfall considering that the two forms of precipitation appear as distinct in Eqs. (2) and (1). Usually only precipitation totals and air temperature are available from meteorological stations. A common procedure for separating rain and snow is to use a threshold air temperature T_s: all the precipitation is considered snow if the air temperature for the time interval is less than or equal to T_s; all the precipitation is considered to be rain if air temperature is greater than T_s. As proposed in Kavetski et al. (2006), to avoid problems for parameter calibration, a smoother filter for thresholds is applied, and the algorithm to discriminate between rainfall and snowfall can be described as follows:

$$\begin{cases} P_\mathrm{r} = \alpha_\mathrm{r} \cdot \left[\frac{P}{\pi} \cdot \arctan\left(\frac{T - T_\mathrm{s}}{m_1}\right) + \frac{P}{2} \right] \\ P_\mathrm{s} = \alpha_\mathrm{s} \cdot \left[P - P_\mathrm{r} \right] \end{cases}, \tag{4}$$

where P [mm t^{-1}] is measured precipitation, P_r [mm t^{-1}] is the rainfall, P_s [mm t^{-1}] is the snowfall, T_s [C] (C stands for Celsius degree) is the threshold temperature, and m_1 [–] is the parameter controling the degree of smoothing (if $m_1 \to 0$ threshold behavior is simulated). The two coefficients α_r and α_s adjust for measurement errors for rain and snow. Because

different values for different climate regions have been found in prior studies (Forland et al., 1996; Rubel and Hantel, 1999; Michelson, 2004), the two coefficients are considered parameters in the model and are therefore calibrated.

2.2 Snowmelt fluxes

The model includes three snowmelt formulae. The user is able to select any of these depending on the site characteristics and data availability.

The first melt component (C1) is a traditional temperature index method where the snowmelt rates depends only on air temperature:

$$M = \begin{cases} \alpha_{\mathrm{m1}} \cdot (T - T_{\mathrm{m}}) & T > T_{\mathrm{m}} \\ 0 & T \leq T_{\mathrm{m}} \end{cases}, \quad (5)$$

where M [mm t^{-1}] is the melt rate, α_{m1} [mm C^{-1} t^{-1}] is the melt factor, T_{m} [C] is the snow-melting temperature, and T [C] is the air temperature. The model can be used either at hourly or daily time steps if the parameters are calibrated accordingly.

The second snowmelt component (C2) is based on the approach presented in Cazorzi and Dalla Fontana (1996): the melt rate is a function of both shortwave radiation and air temperature. The equation for melt during the day is

$$M = \begin{cases} \alpha_{\mathrm{m2}} \cdot EI \cdot (T - T_{\mathrm{m}}) \cdot V_{\mathrm{S}} & T > T_{\mathrm{m}} \\ 0 & T \leq T_{\mathrm{m}} \end{cases}. \quad (6)$$

The equation for the melt process during the night is

$$M = \begin{cases} \alpha_{\mathrm{m2}} \cdot \min(EI) \cdot (T - T_{\mathrm{m}}) \cdot V_{\mathrm{S}} & T > T_{\mathrm{m}} \\ 0 & T \leq T_{\mathrm{m}} \end{cases}, \quad (7)$$

where α_{m2} [mm C^{-1} t^{-1} E^{-1}] is the combined melt factor, and E stands for W m^{-2}; EI [E t^{-1}] is an energy index, and V_{S} [–] is the sky view factor. The energy index is the mean energy from shortwave radiation over a given period at a certain point, and can be variable in space. In practice, the shortwave direct and diffuse solar radiation is estimated by means of an appropriate tool. In this paper, as presented in Cazorzi and Dalla Fontana (1996), five EI maps are computed starting from 21 December (winter solstice) to the middle of February, March, April, May and June. Different time intervals could be selected depending on user needs. During the night the snowmelt is a function of the energy index minimum value of the considered map, as presented in Cazorzi and Dalla Fontana (1996).

The third snowmelt component (C3) is based on the formula presented in Hock (1999). Unlike C2, where the energy index is variable in space but integrated over time, C3 requires the computation of the solar energy for each time step of the simulation. The melt formula is

$$M = \begin{cases} (\alpha_{\mathrm{m3}} + \alpha_e \cdot R_{\mathrm{s}}(t)) \cdot V_{\mathrm{S}} \cdot (T - T_{\mathrm{m}}) & T > T_{\mathrm{m}} \\ 0 & T \leq T_{\mathrm{m}} \end{cases}, \quad (8)$$

where $R_{\mathrm{s}}(t)$ [E] is the incoming (beam plus diffuse) solar radiation received by the pixel and computed using the model presented in Formetta et al. (2013), α_e [mm C^{-1} E^{-1} t^{-1}] is the radiation factor and α_{m3} [mm C^{-1} t^{-1}] is the melt factor. The shortwave radiation model from Formetta et al. (2013), unlike the radiation model presented in the original Hock's formula, is able to account for shadow effects and complex topography and to compute diffuse radiation.

2.3 Freezing

The rate of freezing F used in the mass balance equations is a linear function of air temperature when the air temperature is less then the melting temperature T_{m}, as presented in Eq. (9).

$$F = \begin{cases} \alpha_{\mathrm{f}} \cdot (T_{\mathrm{m}} - T) & T < T_{\mathrm{m}} \\ 0 & T \geq T_{\mathrm{m}} \end{cases}, \quad (9)$$

where F [mm t^{-1}] is the freezing rate, and α_{f} [mm C^{-1} t^{-1}] is the freezing factor.

For both melt and freezing, if the model is run at a daily time step, temperature is the mean daily temperature. If it is applied at and hourly time step, temperature is the mean hourly temperature.

3 SWE-C integration in the NewAge-JGrass system

The NewAge-JGrass system (Formetta, 2013) provides a pool of model components that can be connected and exchanged at runtime. A working set of components constitutes a modeling solution (MS) which is usually set up for a particular purpose or set of simulations. An MS is actually tied together by means of a scripting language (a domain-specific language or DSL), and the scripts can be stored together with the input data to preserve the memory of a certain simulation set, which can then be easily reproduced and inspected by third parties. NewAge-JGrass includes components that simulate various hydrological processes, such as

- the space–time structure of precipitation (KRIGING);
- shortwave and long-wave radiation balance, (SWRB and LWRB) (Formetta et al., 2013);
- evapotranspiration (Priestley–Taylor or Penman–Monteith);
- runoff production (Hymod) (Formetta et al., 2011);
- aggregation and routing of flows in channel (Routing) (Formetta et al., 2011);
- model evaluation component (NewAge-V).

Finally, it also includes three different automatic calibration algorithms:

– particle swarm optimization component (Eberhart and Shi, 2001);

– Let us calibrate (LUCA) component (Hay et al., 2006);

– Differential Evolution Adaptive Metropolis (DREAM) component (Vrugt et al., 2009).

The system is based on a hillslope-link geometrical partition of the landscape, so the basic unit for the water budget evaluation is the hillslope. Each hillslope, rather than a cell or a pixel, drains into a single associated link. The model requires interpolation of the meteorological forcing data (air temperature, precipitation, relative humidity) for each hillslope. This operation can be handled by a deterministic inverse distance weighted algorithm (Cressie, 1992; Lloyd, 2005), kriging (Goovaerts, 1997) or detrended kriging as in Garen et al. (1994) and Garen and Marks (2005).

The radiation model (Formetta et al., 2013) implements algorithms that take into account shadows and complex topography. Shortwave radiation under generic sky conditions (all-sky) is computed according to Helbig et al. (2010) and using different parameterization choices such as Erbs et al. (1982), Reindl et al. (1990) and Orgill and Hollands (1977). The long-wave radiation budget is based on Brutsaert (1982) and Brutsaert (2005).

All modeling components (including those not described here) can be calibrated using one of the automatic calibration algorithms implemented: the particle swarm optimization algorithm, LUCA and DREAM. Evaluation of each model component's behavior is eventually carried out with the use of NewAge-V (verification/validation), which provides some of the classical indices of goodness of fit, such as Nash–Sutcliffe, percent bias, index of agreement and Kling–Gupta efficiency, all defined in Appendix A. The complete interoperating set of components available so far can be seen in Fig. 1.

The snowmelt model components, SWE-C, are perfectly integrated into the NewAge System as presented in Fig. 2. It uses the kriging tools for spatial interpolation of temperature and precipitation and another interpolation method, JAMI (Just Another Meteo Interpolator), presented in Formetta (2013) for temperature interpolation. Like the interpolation algorithms, SWE-C can be applied both to raster grids and to individual points. SWE-C also uses the NewAge shortwave radiation component to estimate the maps of accumulated energy in different periods of the year based on topography, shadow and cloud cover. The SWE-C outputs could be raster maps or time series of snow water equivalent and snowmelt for any point within the domain. If coupled with runoff modeling, these points could be centroids of hillslopes. The SWE-C component could be connected to the NewAge and OMS3 calibration algorithm to estimate the best model parameter values.

The MS shown in Fig. 2 can be further connected to other available components to obtain an estimation of the runoff,

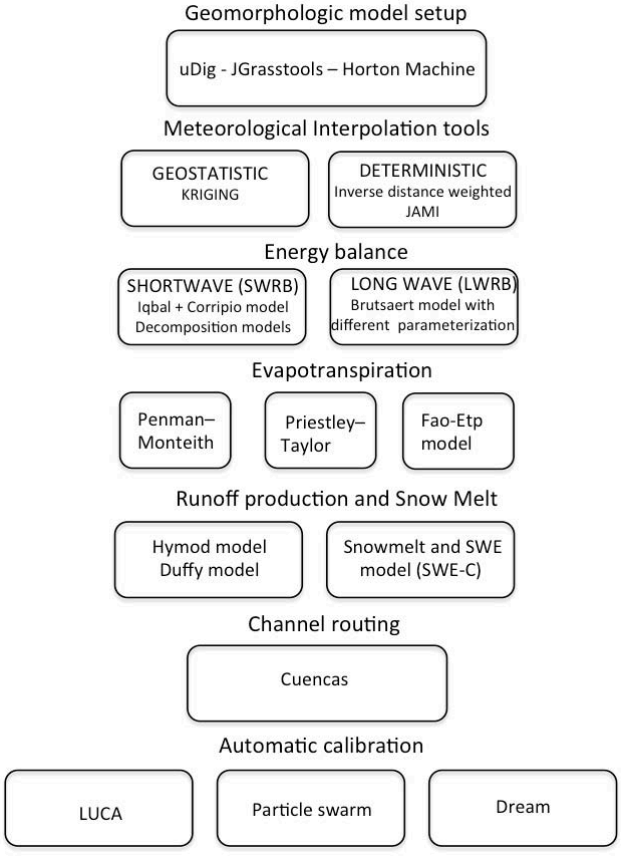

Fig. 1. The NewAge system showing all the modeling components, starting from the top: the uDig Geographic Information System (GIS), the meteorological data interpolation tools, energy balance, evapotranspiration, runoff production-routing and snow water equivalent. The user can select and connect different components and use automatic calibration algorithms (at the bottom) to optimize model parameters.

although demonstration of this application is not the goal of this paper.

4 NewAge-SWE evaluation

4.1 Sites and data description

To test the performance of SWE-C, the model is applied in the upper Cache la Poudre River basin, located in the Rocky Mountains of northern Colorado and southern Wyoming, USA. This basin is 2700 km^2 and has elevations ranging from 1590 to 4125 m, with mean annual precipitation ranging from 330 mm at lower elevations to 1350 mm at the highest elevations (Richer et al., 2013).

Six meteorological stations have precipitation and temperature data in this river basin. These stations are presented in Fig. 3, and Table 1 shows their main features. The Hourglass, Deadman Hill and Joe Wright stations are part of the Natural

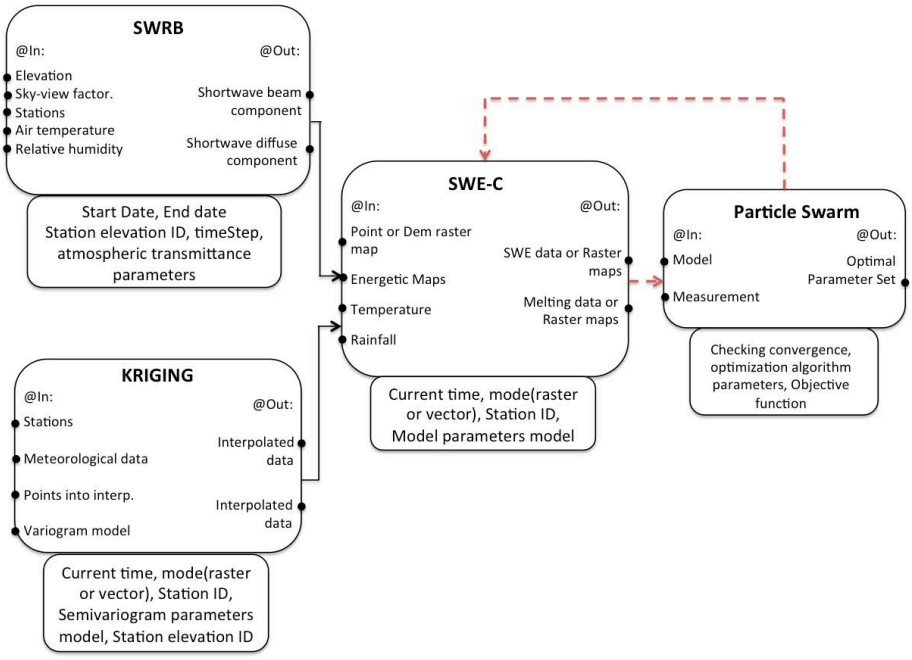

Fig. 2. The SWE-C integration into the NewAge system, showing connections with the shortwave radiation component and kriging interpolation algorithm. The connection with the particle swarm optimization algorithm is presented as a red dashed line.

Table 1. Meteorological stations used in test simulations for the Cache la Poudre River basin.

Station	Lat.	Long.	Elevation (m)
Hourglass	40.25	105.38	2814
Joe Wright	40.32	105.53	3085
Deadman Hill	40.40	105.46	3115
Buckhorn Mountain	40.60	105.28	2256
Virginia Dale	40.95	105.21	2138
Rustic	40.70	105.70	2347

Resource Conservation Service Snow Telemetry (SNOTEL) network. They provide data (precipitation, air temperature and SWE) at a daily time step. For the Hourglass station the data used start on 1 October 2008 and end on 1 October 2013. For the Joe Wright and Deadman Hill stations, the data used start on 1 October 1999 to 1 October 2013. For the Joe Wright station, hourly time series of precipitation, air temperature and snow water equivalent were also available from 1 October 2008 to 1 October 2013.

The Buckhorn Mountain, Rustic and Virginia Dale stations are part of the National Weather Service Cooperative Observer Program (COOP). They only provide precipitation and air temperature, not SWE. For these three stations, data from 1 October 2008 to 1 October 2009 were used for air temperature and precipitation interpolations in the fully distributed application of the snow model.

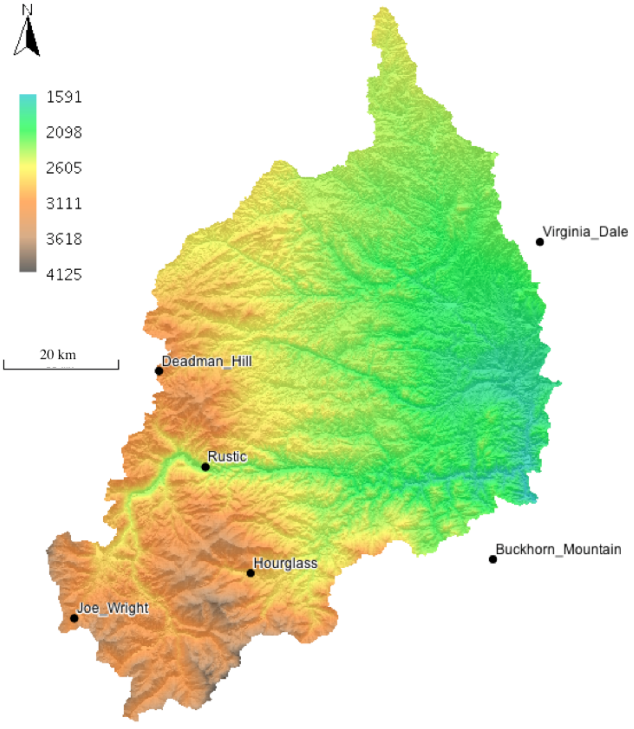

Fig. 3. Cache la Poudre River basin digital elevation model. Elevations are in meters.

Table 2. Optimal parameter values estimated for each of the three SNOTEL stations for the C1 model at a daily time step.

	α_{m1} [mm C^{-1} d^{-1}]	α_r [–]	α_s [–]	α_f [mm C^{-1} d^{-1}]	T_m [°C]	α_l [–]
Hourglass	0.96	1.01	1.35	3.0×10^{-4}	-1.24	0.38
Joe Wright	2.68	1.13	0.98	1.0×10^{-4}	-0.03	0.14
Deadman Hill	1.86	1.25	0.98	1.8×10^{-4}	1.65	0.44

Table 3. Optimal parameter values estimated for each of the three SNOTEL stations for the C2 model at a daily time step. E is in W m^{-2}.

	α_{m2} [mm C^{-1} E^{-1} d^{-1}]	α_r [–]	α_s [–]	α_f [mm C^{-1} d^{-1}]	T_m [°C]	α_l [–]
Hourglass	0.32	1.28	1.01	1.24×10^{-4}	1.64	0.70
Joe Wright	0.50	1.17	1.12	0.002	1.51	0.03
Deadman Hill	0.22	1.29	1.025	0.01	−0.49	0.61
Multisite	0.27	1.13	0.93	0.09	1.62	0.30

4.2 Use of the data and setup of the simulations

Three applications were performed: simulation of SWE at a daily (Test n.1) and hourly (Test n.2) time step and model application in distributed mode (Test n.3). Calibration of SWE-C was conducted within the NewAge-JGrass system shown in Fig. 2 using the particle swarm calibration algorithm. The first year of the available time series was selected as the calibration period for each station. The "optimal" parameter set estimated in the calibration period was used for the model application in the remaining part of the available time series (evaluation period). The concept of equifinality is an important consideration in hydrologic models, where multiple parameters sets can produce the same simulation outcome (Beven, 2006) and it is possible that the optimal parameter sets identified are non-unique. This issue of parameter uncertainty can be addressed in the NewAge-JGrass modeling platform, which includes an omsGLUE (Generalized Likelihood Uncertainty Estimation) component (Beven and Binley, 1992) for estimating model parameter uncertainty. This component models a process by simply requiring the specification of its parameters' lower and upper bounds. After a user-defined number of simulations with different parameter sets, it splits the results into behavioral and non-behavioral following the approach of Beven (1993) and Beven (2001), using a suitable threshold value of a goodness of fit measure.

The Kling–Gupta efficiency (KGE), see Appendix, presented in Gupta et al. (2009), was selected as the calibration objective function. The appendix also describes the motivation for selecting the goodness of fit indices used in the paper and presents equations for each: Nash–Sutcliffe efficiency (NSE), percentage bias (PBIAS) and index of agreement (IOA).

4.3 Test 1: model calibration and evaluation at daily time step

In this application, models C1 and C2 were calibrated and verified. Model C3 was not applied in this case because the SWRB component needed air temperature and relative humidity at an hourly time step to compute the incoming solar radiation. As specified in Formetta et al. (2013), this is necessary for modeling the current atmospheric transmittances. This information was not available at every station. Tables 2 and 3 report the optimal parameter sets of the models C1 and C2, respectively, for each of the three locations where they were applied.

Tables 4 and 5 show the goodness of fit values for the models C1 and C2, respectively, for the calibration period, for the entire simulation period and for the three SNOTEL stations. Model C2 performs better than the classical temperature index model both in the calibration and in the evaluation period in each of the three locations.

Values of the objective function, KGE, were around 0.90 for the model C1 and around 0.95 for model C2, for the calibration periods. In the evaluation period, values decreased to 0.80 for model C1 and 0.90 for C2. Similarly, values of the other performance metrics declined from the calibration to evaluation time periods, but they are all within the range specified for "good" model performance according the guidelines presented in Stehr et al. (2008) and Van Liew et al. (2005). Thus, in each of the three locations the model performance (C1 and C2) deteriorates in the evaluation period.

The performance decrease is much more evident for the C1 model. This may be because the model computes melt as a function of only temperature and a melt parameter, whereas C2 also incorporates EI and V_S.

In the application for the Deadman Hill location, Fig. 4, the two models perform similarly in most years, but in

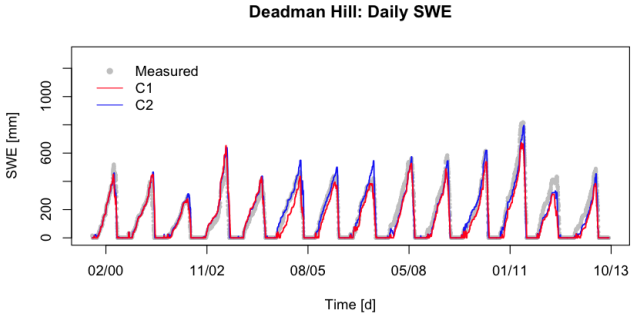

Fig. 4. Calibration and evaluation model results for the station-specific calibration test at the Deadman Hill station: the gray dots represent the measured SWE, the solid red line represents the model C1 (classical temperature index model) and the blue solid line represents the model C2 (Cazorzi and Dalla Fontana).

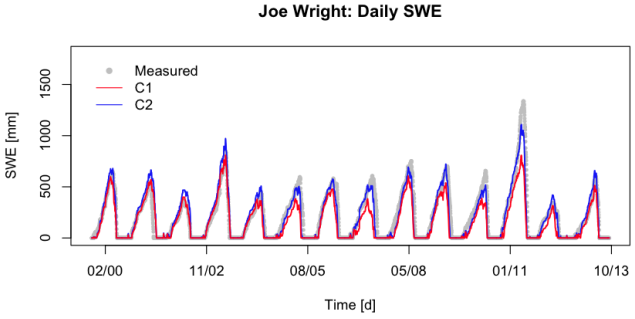

Fig. 5. Calibration and evaluation model results for the station-specific calibration test at the Joe Wright station: the gray dots represent the measured SWE, the solid red line represents the model C1 (classical temperature index model) and the blue solid line represents the model C2 (Cazorzi and Dalla Fontana).

several years (i.e., 2004–2006) the C1 model (classical temperature index) underpredicts SWE, potentially suggesting a stronger role of shortwave radiation in providing melt energy for those years. The applications at the Joe Wright and Hourglass sites, Figs. 5 and 6, respectively, show higher sensitivity in the C2 model, which generally has a higher peak SWE.

For any of these applications, all parameters related to snow accumulation and melt have been optimized, so it is not possible to determine whether differences between the performance of the melt models are related primarily to the model structure or to the parameter combination selected in the optimization algorithm.

4.4 Test 2: SWE hourly simulations: model intercomparison

In this application the three snowmelt components (C1, C2 and C3) were calibrated and verified against measured data. This can be done with regard to the Joe Wright station, where air temperature, rainfall and snow water equivalent at hourly time steps were available. The NewAge OMS component

Table 4. Goodness of fit values for the calibration (top) and evaluation periods (bottom) for the site-specific calibrations at three SNOTEL stations and for the model C1 at a daily time step.

Period	Station	KGE	NSE	PBIAS	IOA
Calibration	Hourglass	0.89	0.91	3.2	0.97
Calibration	Joe Wright	0.88	0.93	−9.1	0.98
Calibration	Deadman Hill	0.90	0.93	−8.6	0.98
Evaluation	Hourglass	0.80	0.82	−11.1	0.95
Evaluation	Joe Wright	0.77	0.71	−21.6	0.91
Evaluation	Deadman Hill	0.81	0.87	−12.9	0.95

Table 5. Goodness of fit values for the calibration (top) and evaluation periods (bottom) for the site-specific calibrations at three SNOTEL stations and for the model C2 at a daily time step.

Period	Station	KGE	NSE	PBIAS	IOA
Calibration	Hourglass	0.98	0.99	2.2	0.99
Calibration	Joe Wright	0.94	0.96	4.9	0.99
Calibration	Deadman Hill	0.97	0.97	1.6	0.99
Evaluation	Hourglass	0.91	0.85	−4.3	0.96
Evaluation	Joe Wright	0.89	0.81	−6.1	0.94
Evaluation	Deadman Hill	0.90	0.85	−2.2	0.95

SWRB (Formetta et al., 2013) was used to estimate incoming solar radiation time series as input to the C3 component. In this case, the calibration period was 2008, and the evaluation period was from 2009 to 2013.

Table 6 presents the optimal parameter set for each component (C1, C2 and C3). For the T_m parameters, it identifies optimal negative values for models C1 and C2 and the optimal positive value for model C3. The values are in line with the value found in Kokkonen et al. (2006). The freezing coefficient, α_f, assumes an optimal value between 0.00850 and 0.0099 [mm C^{-1} h^{-1}] for the three models. The coefficients for snow (α_s) and rainfall (α_r) precipitation are in line with the range estimated in the literature (Forland et al., 1996, and Rubel and Hantel, 1999).

Table 7 present the indices of goodness of fit for the calibration and evaluation periods of each model. Finally, Fig. 7 presents the comparison between simulated and observed snow water equivalent for the three models. The gray dots are the measured data, and green, red and blue solid lines are the data modeled by using the C1, C2 and C3 component, respectively.

From the plot in Fig. 7 and the analysis of Table 7, it is clear that the three models are able to capture the variation in time of the snow water equivalent. Moreover, similar to the daily time step application, the performance of the three models deteriorates in the evaluation period. C2 is the best at preserving the goodness of fit, whereas C1 and C3 are the models that better capture the snow water equivalent for the

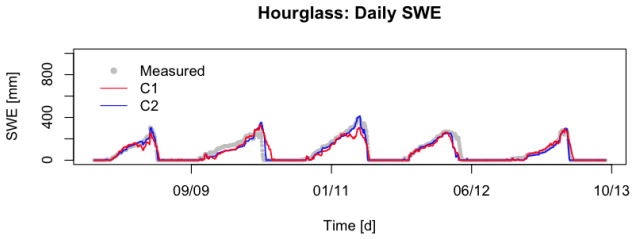

Fig. 6. Calibration and evaluation model results for the station-specific calibration test at the Hourglass station: the gray dots represent the measured SWE, the solid red line represents the model C1 (classical temperature index model) and the blue solid line represents the model C2 (Cazorzi and Dalla Fontana).

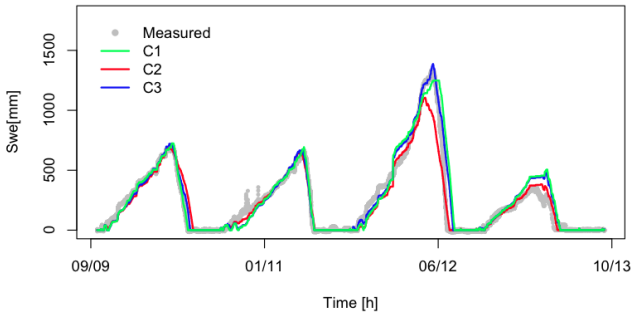

Fig. 7. SWE-C application with an hourly time time step at the Joe Wright station. The gray dots are the measured data, and green, red and blue solid lines are the data modeled by using the C1, C2 and C3 components, respectively.

calibration period and for the 2012 portion of the time series shown in Fig. 7. In the last event (2013) in Fig. 7, models C1 and C3 overestimate peak snow water equivalent, whereas C2 has a stronger performance. The timing of the complete melting of the snow is well simulated by the three models, with Cazorzi and Dalla Fontana's model (C2) performing the best of the three in the evaluation period

Finally, hourly SWE data as available on the website http://www.wcc.nrcs.usda.gov/snow/ are shown in Fig. 7. The plot of measured snow water equivalent data shows how difficult it is to collect accurate measurements at an hourly time step: instability of the signal is evident in 2011 and 2013. Models, even ones as simple as those presented in this paper, could provide help in identifying data errors.

4.5 Test 3: distributed application of SWE-C

The aim of this application is to show that the SWE-C component is able to produce snow water equivalent maps. Moreover, the full integration in the NewAge JGrass system allows the user to immediately visualize and manage output raster maps. The SWE-C model is tested in distributed mode for the entire Cache la Poudre Basin by using the C2 component. The simulation period was between 1 October 2008 and 1 October 2009. Daily rainfall and temperature raster

Table 6. Optimal parameter values estimated for the Joe Wright station for models C1, C2 and C3. E is in $\mathrm{W\,m^{-2}}$.

Parameter	Units	Model C1	Model C2	Model C3
α_{m1}	$[\mathrm{mm\,C^{-1}\,h^{-1}}]$	0.0678	[–]	[–]
α_{m2}	$[\mathrm{mm\,C^{-1}\,E^{-1}\,h^{-1}}]$	[–]	0.0085	[–]
α_{m3}	$[\mathrm{mm\,C^{-1}\,h^{-1}}]$	[–]	[–]	0.07
α_e	$[\mathrm{mm\,C^{-1}\,E^{-1}\,h^{-1}}]$	[–]	[–]	4.8×10^{-5}
α_r	[–]	0.81	1.32	1.50
α_s	[–]	0.83	1.10	0.81
α_f	$[\mathrm{mm\,C^{-1}\,h^{-1}}]$	0.0098	0.0099	0.0085
T_m	[C]	−0.31	−1.5	1.1
α_l	[–]	0.80	0.43	0.54

Table 7. Goodness of fit values for the calibration (top) and evaluation periods (bottom) for the site-specific calibrations at the Joe Wright station and for the models C1, C2 and C3 at an hourly time step.

Period	Model	KGE	NSE	PBIAS	IOA
Calibration	C1	0.97	0.99	2.7	0.99
Calibration	C2	0.95	0.93	1.7	0.98
Calibration	C3	0.98	0.97	1.2	0.99
Validation	C1	0.85	0.86	4.8	0.97
Validation	C2	0.90	0.91	6.1	0.98
Validation	C3	0.86	0.90	7.3	0.98

maps were computed using the detrended kriging algorithm. In this case three SNOTEL and three COOP meteorological stations were used (Table 1). Ideally, more than six meteorological stations are required in order to perform a robust estimation of the variogram for kriging application. NewAge-JGrass also offers the possibility to switch interpolation algorithms and includes an inverse distance weighted option

In order to estimate the parameter set for the distributed simulation, a multisite calibration for the year 2008 was performed. The particle swarm algorithm was applied for simultaneously optimizing the objective function defined in Eq. (10):

$$\overline{\mathrm{KGE}} = \mathrm{KGE_J} + \mathrm{KGE_H} + \mathrm{KGE_D}, \quad (10)$$

where $\mathrm{KGE_J}$, $\mathrm{KGE_H}$ and $\mathrm{KGE_D}$ are the Kling–Gupta efficiency evaluated at the Joe Wright, Deadman Hill and Hourglass sites, respectively, for the calibration period. Table 3, at the bottom, presents the parameter values.

Simulated SWE distributions for select dates are presented in Fig. 8. Snow water equivalent maps were plotted for each month starting from 1 December 2008 to 1 April 2009, and seven classes of snow water equivalent values are plotted for each month in Fig. 8. The dynamics of the snow accumulation and melt are consistent with the model structure and expected seasonal pattern of snow, where the snow accumulation increases with elevation and peaks in spring. However, the number of stations used to compute daily precipitation

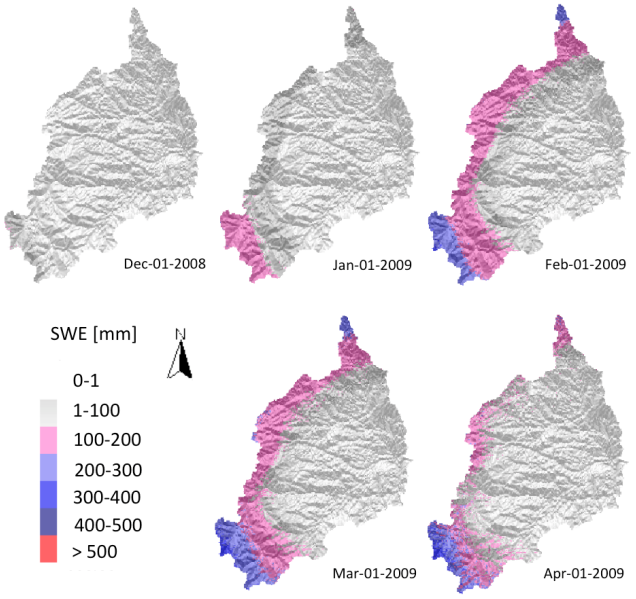

Fig. 8. SWE-C application in distributed mode: snow water equivalent maps from 1 November to 1 June for the upper Cache la Poudre Basin.

and temperature maps was relatively small, and further work is needed to test how the simulated SWE patterns compare to observations. Future work will compare these simulated SWE patterns to a more complex distributed model simulation of SWE and to satellite-derived snow cover patterns.

5 Conclusions

This paper presents a parsimonious snow water equivalent model based on water and ice mass balance. The model simulates snowmelt using one of three separate temperature-based formulae where melt rates are a function of either temperature only or both temperature and solar radiation. The model is integrated into the NewAge-JGrass hydrological model as an OMS3 component, and for this reason it can make use of all the OMS3 components of the system: GIS-based visualization, automatic calibration algorithm and evaluation packages. All of these components are applied and verified at three SNOTEL stations located in the Cache la Poudre River basin (Colorado, USA), and the model performs well for both daily and hourly time steps, although model performance degrades from the calibration to the evaluation periods. This is much more evident at a daily time step compared to an hourly time step. This outcome suggests that both the degree-day and the enhanced degree-day models are very sensitive to the parameter values. Furthermore, they have to be evaluated not only for their performance at individual sites but also for their ability to simulate SWE over time and space.

Using an hourly time step reduces the model performance degradation when moving from the calibration to the evaluation period. Therefore, a possible way to improve forecasting could be to adopt a time-varying degree-day factor as in Tobin et al. (2013).

Finally, the model is applied in distributed mode to simulate spatial patterns of SWE across the basin. Modeling snow water equivalent patterns in a distributed mode provides the possibility to compare them with more physically based snow models and the option to verify them with snow water equivalent remote sensing data. Future research will address problems related to modified temperature index snow water equivalent models such as the transferability of parameter values to new locations and time periods, over-parameterization, comparison with physically based snow models and the evaluation of how well simulated snow cover spatial patterns reproduce spatial and temporal variability of the snowpack.

Appendix A

Objective function and goodness of fit quantifiers

The Kling–Gupta efficiency (KGE), Eq. (A1), presented in Gupta et al. (2009), was selected as the calibration objective function.

KGE, unlike other goodness of fit indices, such as the Nash–Sutcliffe efficiency, is able to synthesize in one objective function three different components from measured (M) and simulated (S) data: (i) correlation coefficient (r), (ii) variability error ($a = \sigma_S/\sigma_M$) and (iii) bias error ($b = \mu_S/\mu_M . \mu_S$); μ_M are the mean values of measured and simulated time series, and σ_S and σ_M are the standard deviations of measured and simulated time series.

$$\mathrm{KGE} = 1 - \sqrt{(r-1)^2 + (a-1)^2 + (b-1)^2} \tag{A1}$$

Three classical goodness of fit indices were computed for each simulation: Nash–Sutcliffe coefficient of efficiency (NSE), percent bias (PBIAS) and index of agreement (IOA). NSE, defined in Eq. (A2), is widely used in assessing the performance of hydrological models. It ranges between $(-\infty, 1)$ and 1 is its best value. While recent studies demonstrate that NSE is not very appropriate to test models with a very strong annual cycle (Schaefli and Gupta, 2007), this metric is used to maintain consistency with the prior studies of Stehr et al. (2008) and Van Liew et al. (2005).

$$\mathrm{NSE} = 1 - \frac{\sum_i (M_i - S_i)^2}{\sum_i (M_i - \mu_M)^2} \tag{A2}$$

The PBIAS is defined in Eq. (A3). The optimal PBIAS value is 0.0. Positive values indicate an overestimation of the model, and negative values represent an underestimation.

$$\mathrm{PBIAS} = 100 \cdot \frac{\sum_i (S_i - M_i)}{\sum_i M_i} \tag{A3}$$

The IOA, proposed by Willmott (1981) and defined in Eq. (A4), varies between 0 and 1. The value 1 indicates a perfect match between observed and simulated time series.

$$\mathrm{IOA} = 1 - \frac{\sum_i (S_i - M_i)^2}{\sum_i (|S_i - \mu_M| + |M_i - \mu_M|)^2} \tag{A4}$$

Following the guidelines in Stehr et al. (2008) and Van Liew et al. (2005), NSE values greater than 0.75 mean that the model can be considered "good"; values between 0.75 and 0.36 are associated with a "satisfactory" model performance; and values below 0.36 indicate a model that is "not satisfactory". A model with an absolute PBIAS value of less then 20 is "good"; if the values are between 20 and 40 it is considered "satisfactory"; and if it is greater than 40 the model is considered "not satisfactory".

Model availability

The stable version of the model used in this paper will be available under a General Public License (GPL) version 3 at: http://code.google.com/p/jgrasstools/. The research version used in this paper is available at https://github.com/formeppe?tab=repositories.

Supplementary material related to this article is available online at http://www.geosci-model-dev.net/7/725/2014/gmd-7-725-2014-supplement.pdf.

Acknowledgements. This study was supported by the project "HydroAlp" financed by Provincia Autonoma di Bolzano, Alto Adige, Ripartizione Diritto allo Studio, Università e Ricerca Scientifica.

Edited by: J. Neal

References

Beven, K.: Prophecy, reality and uncertainty in distributed hydrological modelling, Adv. Water Res., 16, 41–51, 1993.

Beven, K.: How far can we go in distributed hydrological modelling?, Hydrol. Earth Syst. Sci., 5, 1–12, doi:10.5194/hess-5-1-2001, 2001.

Beven, K.: A manifesto for the equifinality thesis, J. Hydrol., 320, 18–36, 2006.

Beven, K. and Binley, A.: The future of distributed models: model calibration and uncertainty prediction, Hydrol. Process., 6, 279–298, 1992.

Brubaker, K., Rango, A., and Kustas, W.: Incorporating radiation inputs into the snowmelt runoff model, Hydrol. Process., 10, 1329–1343, 1996.

Brun, E., David, P., Sudul, M., and Brunot, G.: A nutnerical tnodel to silDulate snow-cover stratigraphy for operational avalanche forecasting, J. Glaciol., 38, 13–22, 1992.

Brutsaert, W.: Evaporation into the atmosphere: Theory, history, and applications, Vol. 1, Springer, 1982.

Brutsaert, W.: Hydrology: an introduction, Cambridge Univ. Press, 2005.

Cazorzi, F. and Dalla Fontana, G.: Snowmelt modelling by combining air temperature and a distributed radiation index, J. Hydrol., 181, 169–187, 1996.

Cressie, N.: Statistics for spatial data, Terra Nova, 4, 613–617, 1992.

Dall'Amico, M., Endrizzi, S., Gruber, S., and Rigon, R.: A robust and energy-conserving model of freezing variably-saturated soil, The Cryosphere, 5, 469–484, doi:10.5194/tc-5-469-2011, 2011.

David, O., Ascough II, J., Lloyd, W., Green, T., Rojas, K., Leavesley, G., and Ahuja, L.: A software engineering perspective on environmental modeling framework design: The Object Modeling System, Environ. Model. Softw., 39, 201–213, 2013.

Eberhart, R. and Shi, Y.: Particle swarm optimization: developments, applications and resources, in: Proceedings of the 2001 congress on evolutionary computation, Vol. 1, 81–86, Piscataway, NJ, USA, IEEE, 2001.

Endrizzi, S.: Snow cover modelling at a local and distributed scale over complex terrain, Ph.D. thesis, Ph. D. dissertation, Dept. of Civil and Environmental Engineering, University of Trento, Italy, 2007.

Endrizzi, S., Gruber, S., Dall'Amico, M., and Rigon, R.: GEOtop 2.0: simulating the combined energy and water balance at and below the land surface accounting for soil freezing, snow cover and terrain effects, Geosci. Model Dev. Discuss., 6, 6279–6341, doi:10.5194/gmdd-6-6279-2013, 2013.

Erbs, D., Klein, S., and Duffie, J.: Estimation of the diffuse radiation fraction for hourly, daily and monthly-average global radiation, Sol. Energ., 28, 293–302, 1982.

Forland, E. J., Allerup, P., Dahlstrom, B., Elomaa, E., Jonsson, T., Madsen, H., Perala, J., Rissanen, P., Vedin, H., and Vejen, F.: Manual for operational correction of Nordic precipitation data, Norwegian Meteorological Institute, 1996.

Formetta, G.: Hydrological modelling with components: the OMS3 NewAge-JGrass system, PhD Thesis, 2013.

Formetta, G., Mantilla, R., Franceschi, S., Antonello, A., and Rigon, R.: The JGrass-NewAge system for forecasting and managing the hydrological budgets at the basin scale: models of flow generation and propagation/routing, Geosci. Model Dev., 4, 943–955, doi:10.5194/gmd-4-943-2011, 2011.

Formetta, G., Rigon, R., Chávez, J. L., and David, O.: Modeling shortwave solar radiation using the JGrass-NewAge system, Geosci. Model Dev., 6, 915–928, doi:10.5194/gmd-6-915-2013, 2013.

Garen, D. and Marks, D.: Spatially distributed energy balance snowmelt modelling in a mountainous river basin: estimation of meteorological inputs and evaluation of model results, J. Hydrol., 315, 126–153, 2005.

Garen, D., Johnson, G., and Hanson, C.: Mean areal precipitation for daily hydrologic modeling in mountainous region, J. Am. Water Resour. As., 30, 481–491, 1994.

Goovaerts, P.: Geostatistics for natural resources evaluation, Oxford University Press, USA, 1997.

Gupta, H., Kling, H., Yilmaz, K., and Martinez, G.: Decomposition of the mean squared error and NSE performance criteria: Implications for improving hydrological modelling, J. Hydrol., 377, 80–91, 2009.

Hay, L., Leavesley, G., Clark, M., Markstrom, S., Viger, R., and Umemoto, M.: Step wise, multiple objective calibration of a hydrologic model for snowmelt dominated basin, J. Am. Water Resour. As., 42, 877–890, 2006.

Helbig, N., Lowe, H., Mayer, B., and Lehning, M.: Explicit validation of a surface shortwave radiation balance model over snow-covered complex terrain, J. Geophys. Res.-Atmos., 115, D18113, doi:10.1029/2010JD013970, 2010.

Hock, R.: A distributed temperature-index ice-and snowmelt model including potential direct solar radiation, J. Glaciol., 45, 101–111, 1999.

Kavetski, D., Kuczera, G., and Franks, S.: Calibration of conceptual hydrological models revisited: 1. Overcoming numerical artefacts, J. Hydrol., 320, 173–186, 2006.

Kokkonen, T., Koivusalo, H., Jakeman, T., and Norton, J.: Construction of a degree–day snow model in the light of the ten iterative steps in model development, in: Proceedings of the iEMSs

Third Biennial Meeting: Summit on Environmental Modelling and Software. Environmental Modelling and Software Society, Burlington, USA, 2006.

Kustas, W. P., Rango, A., and Uijlenhoet, R.: A simple energy budget algorithm for the snowmelt runoff model, Water Resour. Res., 30, 1515–1527, 1994.

Lehning, M., Völksch, I., Gustafsson, D., Nguyen, T. A., Stähli, M., and Zappa, M.: ALPINE3D: a detailed model of mountain surface processes and its application to snow hydrology, Hydrol. Process., 20, 2111–2128, 2006.

Lloyd, C.: Assessing the effect of integrating elevation data into the estimation of monthly precipitation in Great Britain, J. Hydrol., 308, 128–150, 2005.

Marks, D., Domingo, J., Susong, D., Link, T., and Garen, D.: A spatially distributed energy balance snowmelt model for application in mountain basins, Hydrol. Process., 13, 1935–1959, 1999.

Martinec, J.: Snowmelt-runoff model for stream flow forecasts, Nord. Hydrol., 6, 145–154, 1975.

Martinec, J., Rango, A., and Major, E.: The Snowmelt-Runoff Model(SRM) user's manual, 1983.

Martinec, J., Rango, A., Roberts, R., Baumgartner, M. F., and Apfl, G. M.: Snowmelt runoff model (SRM) user's manual, Geographisches Institut der Universität, 1994.

Michelson, D.: Systematic correction of precipitation gauge observations using analyzed meteorological variables, J. Hydrol., 290, 161–177, 2004.

Orgill, J. and Hollands, K.: Correlation equation for hourly diffuse radiation on a horizontal surface, Sol. Energ., 19, 357–359, 1977.

Reindl, D., Beckman, W., and Duffie, J.: Diffuse fraction correlations, Sol. Energ., 45, 1–7, 1990.

Richer, E. E., Kampf, S. K., Fassnacht, S. R., and Moore, C. C.: Spatiotemporal index for analyzing controls on snow climatology: application in the Colorado Front Range, Phys. Geogr., 34, 85–107, 2013.

Rigon, R., Bertoldi, G., and Over, T.: GEOtop: A distributed hydrological model with coupled water and energy budgets, J. Hydrometeorol., 7, 371–388, 2006.

Rubel, F. and Hantel, M.: Correction of daily rain gauge measurements in the Baltic Sea drainage basin, Nord. Hydrol., 30, 191–208, 1999.

Schaefli, B. and Gupta, H. V.: Do Nash values have value?, Hydrol. Process., 21, 2075–2080, 2007.

Stehr, A., Debels, P., Romero, F., and Alcayaga, H.: Hydrological modelling with SWAT under conditions of limited data availability: evaluation of results from a Chilean case study, Hydrolog. Sci. J., 53, 588–601, 2008.

Tarboton, D. G. and Luce, C. H.: Utah energy balance snow accumulation and melt model (UEB), Citeseer, 1996.

Tobin, C., Schaefli, B., Nicótina, L., Simoni, S., Barrenetxea, G., Smith, R., Parlange, M., and Rinaldo, A.: Improving the degree-day method for sub-daily melt simulations with physically-based diurnal variations, Adv. Water Resour., 55, 149–164, 2013.

Van Liew, M., Arnold, J., and Bosch, D.: Problems and potential of autocalibrating a hydrologic model, T. ASAE, 48, 1025–1040, 2005.

Vrugt, J., Ter Braak, C., Diks, C., Higdon, D., Robinson, B., and Hyman, J.: Accelerating Markov chain Monte Carlo simulation by differential evolution with self-adaptive randomized subspace sampling, Int. J. Nonlin. Sci. Num., 10, 273–290, 2009.

Willmott, C. J.: On the validation of models, Phys. Geogr., 2, 184–194, 1981.